

# On-off Charging of Electrical Vehicles in Smart Grids<sup>☆</sup>

Y. Shi<sup>a</sup>, H. D. Tuan<sup>a</sup>, T. Q. Duong<sup>b</sup>, H. V. Poor<sup>c</sup>, A. V. Savkin<sup>d</sup>

<sup>a</sup>*School of Electrical and Data Engineering, University of Technology, Sydney, NSW 2007, Australia*

<sup>b</sup>*School of Electronics, Electrical Engineering and Computer Science, Queen's University Belfast, Belfast BT7 1NN, UK*

<sup>c</sup>*Department of Electrical Engineering, Princeton University, Princeton, NJ 08544, USA*

<sup>d</sup>*School of Electrical Engineering and Telecommunications, the University of New South Wales, NSW 2052, Australia*

---

## Abstract

Massive integration of plug-in electric vehicles (PEVs) into a power grid potentially gives rise to its operating fluctuation, which is not easily controlled due to the unavailability of the PEVs' power demand profiles prior to their random connections to the grid. The present paper considers the problem of joint coordination of PEV charging and grid power control to minimize both PEV charging cost and energy generation cost in meeting both residential and PEVs' power demands and suppressing the potential impact of PEV integration. An on-off PEV charging strategy, under which individual PEVs either charge at a maximal power in on-charging-mode or do not charge at all in off-charging-mode at each of a sequence of time slots, is adopted to exploit its simple online implementation. Based on a recently developed model predictive control [1], which is free from assumptions about the probability distribution of PEV arrivals, knowledge of PEVs future demand, or the unlimited charging capacity of PEVs, a mixed integer nonlinear programming problem (MINP) in binary variables of the PEV charging strategy and continuous variables of the grid voltages is proposed at each time for implementing an online algorithm. Due to the large dimension of the continuous voltage variables and the binary on-off decision variables, this MINP is a large scale optimization problem, which is very computationally challenging. A major contribution of the paper is to develop a new solver for this MINP, which is practical for its online computation. Its capability for achieving an optimal solution is shown by numerical examples.

*Keywords:* Smart power grid, plug-in electric vehicles (PEVs), online algorithm, on-off control, mixed integer nonlinear programming, mixed integer convex programming

---

## 1. Introduction

Significant breakthroughs and innovations in battery and smart vehicle technology have driven the electric-vehicle (EV) boom in the 21st century [2]. Competing against internal-combustion vehicles on both price and performance, EVs are projected to make up 15 to 30 percent of new vehicles by 2030 [3]. EVs can be recharged not only at immobile EV charging stations but also in standard electrical power points at any location and time. It is clear that plug-in EVs (PEVs) should be supported by the future smart grid to gain advantages such as lower operation costs, less toxic emissions and better use of renewable energy [4, 5]. Conventionally, a power grid serves traditional residential power demands, so the massive integration of PEVs could pose potential threats to its stability, which are not easily compensated [6, 7, 8, 9]. Particularly, PEV charging potentially leads to serious overloading, additional power loss, and unacceptable voltage violation in the smart grid

system [10, 11]. The coordination of PEV charging plays a crucial role on reducing the generation costs and EV charging costs and shifting peak load in power system [12, 13]. Research in [14] shows that PEVs have the ability to balance the electricity demand and supply especially for large-scale renewable energy integration. Therefore, there is an increasing need to coordinate PEV charging to offer a cost-saving service in meeting PEV power demands and other consumer power demands.

Coordination of PEV charging/discharging has been studied in recent works such as [15, 16, 17]. Reference [15] aimed to maximize the aggregator's profit under different charging conditions in an unidirectional vehicle-to-grid (V2G) network. A charging and discharging coordination for PEVs using a bidirectional power flow with voltage control on distribution grids was investigated in [16]. Reference [17] aimed to flat the total demand curve with the bidirectional energy flow and proposed a decentralized algorithm for charging and discharging coordination of PEVs. An on-off charging strategy for PEVs, under which individual PEVs either charge at a maximal power in on-charging mode or do not charge at all in off-charging mode at each of a sequence of time slots has gained renewed attention recently due to its easy and efficient on-

---

<sup>☆</sup>Corresponding author H. D. Tuan, Tel. +61 (0)2 9514 9056.

*Email addresses:* ye.shi@student.uts.edu.au (Y. Shi), tuan.hoang@uts.edu.au (H. D. Tuan), trung.q.duong@qub.ac.uk (T. Q. Duong), poor@princeton.edu (H. V. Poor), a.savkin@unsw.edu.au (A. V. Savkin)

line implementation [18, 19, 20]. As the length of the time slots ranges from 30 minutes to an hour, PEVs are also available for engaging other services if they are in the off-charging mode. A mixed integer linear programming problem (MILP) was proposed in [18] to optimize the daily cost of PEV on-off charging under linearized power flow equations. It is not transparent how to compensate the modelling errors due to the equations' linearization. Reference [19] proposed a mixed integer nonlinear programming problem (MINLP) for coordination of PEV on-off charging in an unbalanced distributed system. The MINLP must be then linearized to a MILP using the first order Taylor expansion and piecewise linear approximation. The solution of the latter is not necessarily feasible for the former. In [20], a similar MILP was proposed with V2G charging added to make PEVs bidirectional power sources for mitigating the negative effect at times of peak demand [15]. All coordination algorithms in [15, 16, 17, 18, 19, 20] are offline as they use all information on PEV arrival and departure times and PEVs initial state of charge (SOC) from the beginning. Offline algorithms are hardly practical in PEV charging applications. Individual PEVs randomly connect to the grid with their demands and as such, neither their arrival and departure times nor their charging demands can be known a priori.

Model predictive control (MPC) for PEV charging has emerged as a natural tool to exploit available online information. For instance, it has been employed in [21] for exclusive coordination of PEV charging over a finite time horizon without incorporating grid operation constraints. Additionally, it is based on the assumption that each PEV can be fully charged within only one time slot, which is quite unrealistic due to the physical limitations of charging technology. An MILP over a rolling horizon window for energy storage control was proposed in [22], ignoring voltage operational constraints. Reference [23] presented an MILP-based MPC for coordinating PEV charging in microgrids under bidirectional, unidirectional and one block charging scenarios. The stochastic optimization tool used in [23] is computationally costly.

Our previous work [1] proposed a novel MPC for the joint coordination of PEV charging and grid power control to save service costs for PEVs and the power generation costs in meeting both residential and PEV power demands. Its distinct practicability is that no assumptions are made about the probability distribution of PEV arrivals, knowledge of PEVs' future demand, or the unlimited charging capacity of PEVs. The charging strategy in [1] is analog in the sense that at each time slot, PEVs can be charged by any value of power in their battery capacity range. As such, it needs a mechanism to control this charge value, which is not always practical. The present paper adopts the aforementioned on-off charging for PEVs to exploit its easy and efficient online implementation, which also facilitates easy coordination and planning for other activities. However, in contrast to the analog charging strategy in [1], which requires online computation of a large scale

nonlinear programming problem (NP) on the continuous voltage and PEV charging variables, the on-off strategy requires online computation of a large scale mixed integer nonlinear programming problem (MINP) on the continuous voltage variables and the binary PEV on-off charging decision variables. Thus, the bottleneck for implementing the on-off strategy is online computation for this large scale MINP, which is much more computationally difficult than the large scale NP in [1]. To the authors' best knowledge, there are even no efficient offline computations for large scale MINPs, which are the reason why all the previous works (see e.g. [18, 19, 20, 22, 23] and references therein) in different contexts must either linearize MINPs at the computation stage or utilize MILPs from the modelling stage to end up with MILPs with the aforementioned compromises. The main contribution of the present paper is a development of computational methods to tackle this MINLP, which is new even from the computational viewpoint. In fact, to accomplish the mission, we develop novel techniques to express computationally intractable binary constraints by computationally tractable continuous constraints and to measure the degree of satisfaction of the binary constraints. They are the principal ingredients in developing efficient algorithms for computational solution of this large scale MINP.

The rest of the paper is structured as follows. Section II is devoted to an MINLP-based MPC for the joint coordination of on-off PEV charging and grid power control with analysis on its computational challenges. The main technical contribution of the paper is Section III, which develops a solver for this MINLP. Section IV considers computation of a lower bound of this MINLP. Simulations are provided in Section V, which particularly show that the developed solver is indeed capable of locating an optimal solution as its found optimal value approximates well its lower bound. Section V concludes the paper.

*Notation.* The notation used in this paper is standard. Particularly,  $j$  is the imaginary unit,  $X^H$  is Hermitian transpose of a vector/matrix  $X$ ,  $M \succeq 0$  for a Hermitian symmetric matrix  $M$  means that it is positive semi-definite,  $\text{rank}(M)$  and  $\text{Trace}(M)$  are the rank and trace of a matrix  $M$ , respectively.  $\Re(\cdot)$  and  $\Im(\cdot)$  are the real and imaginary parts of a complex quantity, and  $a \leq b$  for two complex numbers  $a$  and  $b$  is componentwise understood, i.e.  $\Re(a) \leq \Re(b)$  and  $\Im(a) \leq \Im(b)$ . The cardinality of a set  $\mathcal{C}$  is denoted by  $|\mathcal{C}|$ .  $\lceil x \rceil$  is the smallest integer that is not less than  $x$ .

## 2. MPC for joint PEV on-off charging coordination and grid power control

Based in [1], this section proposes an MPC for on-off PVEs charging by a smart grid system and also analyzes its principal computational challenges.

Consider an electric power grid with a set of buses  $\mathcal{N} \triangleq \{1, 2, \dots, N\}$  connected through a set of flow lines  $\mathcal{L} \subseteq \mathcal{N} \times \mathcal{N}$ , under which bus  $k$  is connected to bus  $m$  if and only

if  $(k, m) \in \mathcal{L}$ . Denote by  $\mathcal{N}(k)$  the set of other buses connected to bus  $k$ .  $\mathcal{G} \subseteq \mathcal{N}$  is the set of those buses that are connected to distributed generators (DGs). A bus in  $\mathcal{G}$  is called a generator bus. A bus  $k \notin \mathcal{G}$  is called a load bus. A bus is referred as a charging station (CS) if it has a function to serve PEVs. Let  $\mathcal{C}$  be the set of CSs.

The serving time period of the grid is divided into  $T$  time slots  $\mathcal{T} \triangleq \{1, 2, \dots, T\}$ . The length of a time slot usually ranges from 30 minutes to an hour. The price-inelastic load varies from each time interval  $[t, t + 1]$  according to the residential power demand profile.

From the grid side, let  $y_{km} \in \mathbb{C}$  be the admittance of line  $(k, m)$  and  $V_k(t')$  be the complex voltage at bus  $k$  during the time slot  $t'$  and  $W(t') \triangleq [W_{k,m}(t')]_{(k,m) \in \mathcal{N} \times \mathcal{N}} = [V_k(t')V_m^*(t')]_{(k,m) \in \mathcal{N} \times \mathcal{N}} \in \mathbb{C}^{\mathcal{N} \times \mathcal{N}}$ . Let  $P_k(t')$  and  $Q_k(t')$  be the known real and reactive price-inelastic demands to express the residential power demand, and  $P_{g_k}(t')$  and  $Q_{g_k}(t')$  be the real and reactive powers generated by the generator bus  $k \in \mathcal{G}$ . For  $t' \in \mathcal{T}$ , the following constraints of the range of generated powers by the DGs, of voltage range and phase balance, and of line capacity are standard:

$$\underline{P}_{g_k} \leq P_{g_k}(t') \leq \bar{P}_{g_k}, \quad k \in \mathcal{G}, \quad (1)$$

$$\underline{Q}_{g_k} \leq Q_{g_k}(t') \leq \bar{Q}_{g_k}, \quad k \in \mathcal{G}, \quad (2)$$

$$\underline{V}_k^2 \leq W_{kk}(t') \leq \bar{V}_k^2, \quad k \in \mathcal{N}, \quad (3)$$

$$\Im(W_{km}(t')) \leq \Re(W_{km}(t')) \tan(\theta_{km}^{\max}), \quad (k, m) \in \mathcal{L}, \quad (4)$$

$$|(W_{kk}(t') - W_{km}(t'))y_{km}^*| \leq S_{km}, \quad (k, m) \in \mathcal{L}, \quad (5)$$

where  $\underline{P}_{g_k}$ ,  $\underline{Q}_{g_k}$  and  $\bar{P}_{g_k}$ ,  $\bar{Q}_{g_k}$  are respectively lower and upper physical limits of the real generated and reactive generated powers,  $\underline{V}_k$  and  $\bar{V}_k$  are the lower limit and upper limit of the voltage amplitude, and  $\theta_{k,m}^{\max}$  are given to express the voltage phase balance, while  $S_{km}$  is the upper limit of capacity for line  $(k, m)$ .

Denote by  $\mathcal{H}_k$  the set of those PEVs that arrive at CS  $k$ . Accordingly,  $k_n$  is the  $n$ -th PEV that arrives at CS  $k$ . Each PEV  $k_n$  arrives at  $t_{a,k_n} \in \mathcal{T}$  and requires to be fully charged by its departing time  $t_{k_n,d} \in \mathcal{T}$ . Suppose that  $C_{k_n}$  and  $s_{k_n}^0$  are the battery capacity and initial SOC of PEV  $k_n$  while  $\bar{P}_{k_n}$  is the maximum power that its battery can charge during one time slot. Unlike [1], which allows each PEV to charge a power  $0 \leq P_{k_n}(t') \leq \bar{P}_{k_n}$  during the time slot  $t'$ , we now adopt an on-off charging strategy, under which PEV  $k_n$  either charges the maximal power  $\bar{P}_{k_n}$  ( $P_{k_n}(t') = \bar{P}_{k_n}$ ) or does not charge at all ( $P_{k_n}(t') = 0$ ). Using the binary variables

$$\tau_{k_n}(t') \in \{0, 1\} \quad (6)$$

to model this strategy, i.e. PEV  $k_n$  charges the power  $P_{k_n}(t') = \tau_{k_n}(t')\bar{P}_{k_n}$  during the time slot  $t'$ , the following constraint on the binary variables  $\tau_{k_n}(t')$  must be satisfied to make PEV  $k_n$  fully charged at its departure:

$$\sum_{t'=t_{k_n,a}}^{t_{k_n,d}} u_h \bar{P}_{k_n} \tau_{k_n}(t') \geq C_{k_n}(1 - s_{k_n}^0), \quad (7)$$

Here  $u_h$  is the charging efficiency of the battery. For  $\bar{\tau}_{k_n} = \lceil C_{k_n}(1 - s_{k_n}^0)/u_h \bar{P}_{k_n} \rceil$ , it follows that (11c) is equivalent to the following linear equality constraint on the binary variables  $\tau_{k_n}(t')$ :

$$\sum_{t'=t_{k_n,a}}^{t_{k_n,d}} \tau_{k_n}(t') = \bar{\tau}_{k_n}. \quad (8)$$

For ease of presentation, we set  $\tau_{k_n}(t') = 0$  for  $t' \notin [t_{k_n,a}, t_{k_n,b}]$ , and  $P_{g_k}(t') \equiv 0$  and  $Q_{g_k}(t') \equiv 0$  for  $k \notin \mathcal{G}$ . The supply energy at bus  $k$  is defined as  $E_k(W(t')) \triangleq \sum_{m \in \mathcal{N}(k)} y_{km}^* (W_{kk}(t') - W_{km}(t'))$ , which is obviously a linear function of  $W_{k,m}(t') = V_k(t')V_m^*(t')$  though it is seen as a nonlinear function of the complex voltage variables  $V_k$ . For  $\tau_k(t') = \{\tau_{k_n}(t')\}_{n \in \mathcal{H}_k}$ , the demand energy at  $k \in \mathcal{C}$  is defined as,

$$D_k(\tau_k(t')) = [P_{g_k}(t') - P_{l_k}(t') - \sum_{n \in \mathcal{H}_k} \bar{P}_{k_n} \tau_{k_n}(t')] + j[Q_{g_k}(t') - Q_{l_k}(t')],$$

leading to the following constraint

$$E_k(W(t')) = D_k(\tau_k(t')), k \in \mathcal{C}, \quad (9)$$

which is a mixed integer nonlinear constraint on the binary variables  $\tau_{k_n}(t')$  and continuous complex voltage variables  $V_k(t')$ . On the other hand, the demand energy at  $k \notin \mathcal{C}$  is obviously defined as

$$D_k(t) \triangleq [P_{g_k}(t') - P_{l_k}(t')] + j[Q_{g_k}(t') - Q_{l_k}(t')],$$

leading to the following constraint

$$E_k(W(t')) = D_k(t), k \notin \mathcal{C}, \quad (10)$$

which is a nonlinear constraint on the continuous complex voltage variables  $V_k(t')$ .

By defining the continuous quantities  $\mathcal{W} \triangleq \{W(t')\}$ ,  $P_g(t') = \{P_{g_k}(t')\}_{k \in \mathcal{G}}$ ,  $Q_g(t') = \{Q_{g_k}(t')\}_{k \in \mathcal{G}}$ ,  $R(t') = \{P_g(t'), Q_g(t')\}$ , and  $\mathcal{R} = \{R(t')\}_{t' \in \mathcal{T}}$ , and the binary quantities  $\tau(t') = \{\tau_k(t')\}_{k \in \mathcal{C}}$ , and  $\tau = \{\tau(t')\}_{t' \in \mathcal{T}}$ , the objective function is defined as

$$\mathcal{F}(\mathcal{R}, \tau) = \sum_{(t',k) \in \mathcal{T} \times \mathcal{G}} [f(P_{g_k}(t')) + \sum_{n \in \mathcal{H}_k} \beta_{t'} \tau_{k_n}(t') \bar{P}_{k_n}] + \gamma \sum_{t' \in \mathcal{T}} (\sum_{k \in \mathcal{N}} P_{l_k}(t') + \sum_{k \in \mathcal{C}} \sum_{n \in \mathcal{H}_k} \bar{P}_{k_n} \tau_{k_n}(t') - \bar{P}_{avg})^2,$$

where  $f(P_{g_k}(t'))$  is the cost function of real power generation by DGs, which is linear or quadratic in  $P_{g_k}(t')$ ,  $\beta_{t'}$  is the known PEV charging price during the time slot  $t'$ , and  $\bar{P}_{avg}$  is the averaged power demand over the serving period, which is estimated based on historical data. Different from the objective function in [1], which is the first term for expressing the sum of the energy cost to DGs and charging cost for PEVs, the second term is added to flatten out the total power demand curve in stabilizing the

grid operations.  $\gamma > 0$  is the weighting factor to trade-off the two conflicting objectives.

Similar to [1], this joint PEV charging coordination and voltage control can be formulated as the following control problem over the finite horizon  $[1, T]$

$$\min_{\mathcal{W}, \mathcal{R}, \tau^{PEV}} \mathcal{F}(\mathcal{R}, \tau^{PEV}) \quad (11a)$$

$$\text{s.t. (1) – (5), (6), (8) – (10),} \quad (11b)$$

$$W(t') \succeq 0, \quad \text{rank}(W(t')) = 1, \quad (11c)$$

where the constraint (11c) is needed for legalizing the nonlinear variable changes  $W_{km}(t') = V_k(t')V_m(t')$ . Note that all equations in (11) are not known a priori, for which the conventional MPC [24, 25] is not applicable. Following [26] we address (11) by developing the following predictive model at each time slot  $t$ , which only uses the information available online.

Denote by  $C(t)$  the set of PEVs that need to be charged at  $t$  and ahead. For each  $k_n \in C(t)$ , let  $d_{k_n}(t)$  be its remaining demand for charging by the departure time  $t_{k_n,d}$ . Therefore, the binary variable

$$\tau_{k_n}(t') \in \{0, 1\}, t' \in [t, t_{k_n,d}], k_n \in C(t) \quad (12)$$

must satisfy the following constraints:

$$\sum_{t'=t}^{t_{k_n,d}} u_h \bar{P}_{k_n} \tau_{k_n}(t') \geq d_{k_n}(t), k_n \in C(t). \quad (13)$$

For  $\bar{\tau}_{k_n}(t) \triangleq [d_{k_n}(t)/u_h \bar{P}_{k_n}]$ , constraint (13) is equivalent to

$$\sum_{t'=t}^{t_{k_n,b}} \tau_{k_n}(t') = \bar{\tau}_{k_n}(t), k_n \in C(t). \quad (14)$$

Define  $\Psi(t) = \max_{k_n \in C(t)} t_{k_n,d}$ . At time  $t$  we solve the following MPC over the prediction horizon  $[t, \Psi(t)]$  but then take only  $V(t)$ ,  $R(t)$  and  $\tau(t)$ , which is the snapshot at  $t$  of its solution, for updating online the solution of (11):

$$\min_{\mathcal{W}_P(t), \mathcal{R}_P(t), \tau_P(t)} F_P(\mathcal{R}_P(t), \tau_P(t)) \quad (15a)$$

$$\text{s.t. (12), (14),} \quad (15a)$$

$$(1) – (5), (9) – (10) \quad \text{for } t' \in [t, \Psi(t)], \quad (15b)$$

$$W(t') \succeq 0, \quad \text{for } t' \in [t, \Psi(t)], \quad (15c)$$

$$\text{rank}(W(t')) = 1, \quad \text{for } t' \in [t, \Psi(t)]. \quad (15d)$$

Here and after, the prediction variable

$$\mathcal{W}_P(t) \triangleq \{W(t')\}_{t' \in [t, \Psi(t)]},$$

$$\mathcal{R}_P(t) \triangleq \{P_g(t'), Q_g(t')\}_{t' \in [t, \Psi(t)]},$$

$$\tau_P(t) = \{\tau_{k_n}(t')\}_{k_n \in C(t), t' \in [t, t_{k_n,d}]},$$

and the prediction objective

$$F_P(\mathcal{R}_P(t), \tau_P(t)) \triangleq \sum_{t'=t}^{\Psi(t)} \left( \sum_{k \in \mathcal{G}} f(P_{g_k}(t')) + \sum_{k_n \in C(t)} \beta_t \tau_{k_n}(t') \bar{P}_{k_n} \right) + \gamma \sum_{t'=t}^{\Psi(t)} \left( \sum_{k \in N} P_{l_k}(t') + \sum_{k \in \mathcal{C}} \sum_{n \in \mathcal{H}_k} \bar{P}_{k_n} \tau_{k_n}(t') - \bar{P}_{avg} \right)^2, \quad (16)$$

are defined.

The difficulty of (15) is concentrated on the multiple nonconvex matrix rank-one constraints in (15d) and multiple binary constraints in (12). In the next section, we propose an efficient computational procedure, which also exploits the fact that only the snapshot at  $t$  of the solution of (15) is extracted to update the online solution of (11).

### 3. Two-stage optimization based solver for MINP

Since in the end we need only the snapshot at  $t$  of the solution of the MINLP (15) for updating online the matrix  $W(t)$  and generated power  $R(t)$ , handling the multiple nonconvex matrix rank-one constraints (15d) for all  $t' \in [t, \Psi(t)]$  in (15) is not necessary. We propose the following two-stage optimization scheme to tackle its computation.

In the first optimization stage, we drop the matrix rank-one constraints in (15d) to relax (15) to the following MICP:

$$\min_{\mathcal{W}_P(t), \mathcal{R}_P(t), \tau_P(t)} F_P(\mathcal{R}_P(t), \tau_P(t)) \quad \text{s.t. (15a) – (15c).} \quad (17)$$

Suppose that  $(\hat{\mathcal{W}}_P(t), \hat{\mathcal{R}}_P(t))$  and  $\hat{\tau}_P(t)$  is the optimal solution of (17). If  $\text{rank}(\hat{W}(t')) \equiv 1$ ,  $t' \in [t, \Psi(t)]$ , then  $\hat{V}(t')$  such that  $\hat{W}(t') = \hat{V}(t')\hat{V}^H(t')$  together with  $\hat{R}(t')$  and  $\hat{\tau}_{k_n}(t')$  constitute the optimal solution of MINP (15). Otherwise, we go to the next optimization stage, which substitutes  $\hat{\tau}_{k_n}(t)$  into (15b) to consider the snapshot at  $t$  of (15) only:

$$\min_{W(t), R(t)} F(P_g(t)) \triangleq \sum_{t'=t}^{\Psi(t)} \sum_{k \in \mathcal{G}} f(P_{g_k}(t')) \quad (18a)$$

$$\text{s.t. (1) – (5), (9) – (10) for } t' = t$$

$$\tau_{k_n}(t) = \hat{\tau}_{k_n}(t), \quad (18b)$$

$$W(t) \succeq 0, \text{rank}(W(t)) = 1. \quad (18c)$$

This nonlinear optimization problem, which involves only one matrix rank-one constraint at  $t' = t$  in (18c), can be efficiently computed by our previously developed non-smooth optimization algorithm [27, 26, 28]. To make the paper self-contained, this optimization algorithm will be recalled in Subsection III.B.

The next subsection is devoted to computation for the MICP (17).

### 3.1. Stage I: New computational solution for MICP problem (17)

It is obvious that the main issue is how to handle the binary constraint (12) in the MICP (17). Our previous works [29] and [30] have shown that the exactly penalized optimization, which simultaneously minimize the objective function and maximize the degree of satisfaction of the binary constraints, is appropriate for addressing the MICP (17). The computational efficiency of the exactly penalized optimization is critically dependent on the function used to measure the degree of satisfaction of the binary constraints, and also the computational tractability of the corresponding exactly penalized optimization problem, which is nonconvex. Therefore, we now develop a novel function used to measure the degree of satisfaction of the binary constraints, and also a new path-following computational procedure, which iteratively improves the solution, for the corresponding exactly penalized optimization problem.

First, the following result establishes the equivalence of the binary constraint (12) and a set of continuous constraints.

**Lemma 1.** *Under the linear constraint (14), the binary constraint (12) is equivalent to the following set of continuous constraints:*

$$0 \leq \tau_{k_n}(t') \leq 1, t' \in [t, t_{k_n,d}], k_n \in C(t), \quad (19)$$

$$g(\tau_P(t)) \geq \bar{\tau}(t) \triangleq \sum_{k_n \in C(t)} \bar{\tau}_{k_n}(t), \quad (20)$$

for  $L > 1$  and  $g(\tau_P(t)) \triangleq \sum_{k_n \in C(t)} \sum_{t'=t}^{t_{k_n,d}} \tau_{k_n}^L(t')$ .

*Proof.* Note that  $\tau_{k_n}^L(t') \leq \tau_{k_n}(t') \forall \tau_{k_n}(t') \in [0, 1]$ , so  $g(\tau_P(t)) \leq \sum_{k_n \in C(t)} \sum_{t'=t}^{t_{k_n,d}} \tau_{k_n}(t') = \bar{\tau}(t)$ . Therefore constraint (20) forces  $g(\tau_P(t)) = \bar{\tau}(t)$ , which is possible if and only if  $\tau_{k_n}^L(t') = \tau_{k_n}(t')$ , i.e.  $\tau_{k_n}(t') \in \{0, 1\}$ , implying (12).

Since  $g(\tau_P(t))$  is convex in  $\tau_P(t)$ , constraint (20) is called reverse convex [31]. Also, as  $L$  decreases,  $g(\tau_P(t))$  approaches the linear function  $\sum_{k_n \in C(t)} \sum_{t'=t}^{t_{k_n,d}} \tau_{k_n}(t')$  and as thus the constraint (20) approaches the linear constraint  $\sum_{k_n \in C(t)} \sum_{t'=t}^{t_{k_n,d}} \tau_{k_n}(t') \geq \bar{\tau}(t)$ . However, it does not mean that choosing  $L$  closer to 1 is effective because the function  $g(\tau_P(t)) - \bar{\tau}(t)$  also approaches zero very quickly, making constraint (20) highly empirical. To the authors' best knowledge, Lemma 1 is new. A particular result for  $L = 2$  was obtained in our previous works [29, 30]. Thanks to Lemma 1, we choose  $L = 1.5$  in this paper as it accelerates the convergence of the proposed optimization algorithms.

The following result is a direct consequence of Lemma 1.

**Proposition 1.** *Under the linear constraint (14), the function*

$$g_1(\tau_P(t)) \triangleq \frac{1}{g(\tau_P(t))} - \frac{1}{\bar{\tau}(t)} \quad (21)$$

can be used to measure the degree of satisfaction of the binary constraint (12) in the sense that  $g_1(\tau_P(t)) \geq 0 \forall \tau_{k_n}(t') \in [0, 1]$  and  $g_1(\tau_P(t)) = 0$  if and only if  $\tau_{k_n}(t')$  are binary (i.e. satisfying (12)).

Instead of handling the reverse convex constraint (20), we incorporate the degree of its satisfaction  $g_1$  into the objective in (17), leading to the following penalized optimization problem:

$$\min_{\mathcal{W}_P(t), \mathcal{R}_P(t), \tau_P(t)} \Phi(\mathcal{R}_P(t), \tau_P(t)) \triangleq F_P(\mathcal{R}_P(t), \tau_P(t)) + \mu g_1(\tau_P(t)) \quad \text{s.t.} \quad (14), (15b), (15c), (19), \quad (22)$$

where  $\mu > 0$  is a penalty parameter. This penalized optimization problem is exact for (17) in the sense that for a sufficiently large  $\mu$ , the optimal solution of (22) is also an optimal solution for (17) [32] and thus satisfies  $g_1(\tau_P(t)) = 0$ . To our best knowledge, using the function  $g_1$  defined by (21) to measure the degree of satisfaction of the bilinear constraint (12) instead of the conventional class  $\bar{\tau}(t) - g(\tau_P(t))$  is new as well.

Note that (22) is a minimization of a nonconvex function over a convex set. We now develop a path-following computational procedure for its solution. For this purpose, we firstly develop an upper bounding approximation at a feasible point  $\tau_P^{(\kappa)}(t)$  for (22). As the function  $g(\tau_P(t))$  is convex, it is true that at  $\tau_P^{(\kappa)}(t)$  [31],

$$\begin{aligned} g(\tau_P(t)) &\geq g^{(\kappa)}(\tau_P(t)) \\ &\triangleq g(\tau_P^{(\kappa)}(t)) + \langle \nabla g(\tau_P^{(\kappa)}(t)), \tau_P(t) - \tau_P^{(\kappa)}(t) \rangle \\ &= -(L-1) \sum_{k_n \in C(t)} \sum_{t'=t}^{t_{k_n,d}} (\tau_{k_n}^{(\kappa)}(t'))^L \\ &\quad + L \sum_{k_n \in C(t)} \sum_{t'=t}^{t_{k_n,d}} (\tau_{k_n}^{(\kappa)}(t'))^{L-1} \tau_{k_n}(t'). \end{aligned} \quad (23)$$

Therefore, an upper bounding approximation at  $\tau_P^{(\kappa)}(t)$  for  $g_1(\tau_P(t))$  can be easily obtained as

$$g_1(\tau_P(t)) \leq g_1^{(\kappa)}(\tau_P(t)) \triangleq \frac{1}{g^{(\kappa)}(\tau_P(t))} - \frac{1}{\bar{\tau}(t)} \quad (24)$$

over the trust region

$$g^{(\kappa)}(\tau_P(t)) > 0. \quad (25)$$

Accordingly, at the  $\kappa$ -th iteration we solve the following convex optimization problem to generate the next iterative point  $(\mathcal{W}_P^{(\kappa+1)}(t), \mathcal{R}_P^{(\kappa+1)}(t), \tau_P^{(\kappa+1)}(t))$ :

$$\begin{aligned} \min_{\mathcal{W}_P(t), \mathcal{R}_P(t), \tau_P(t)} \Phi^{(\kappa)}(\mathcal{R}_P(t), \tau_P(t)) &\triangleq \\ F_P(\mathcal{R}_P(t), \tau_P(t)) + \mu g_1^{(\kappa)}(\tau_P(t)) &\quad \text{s.t.} \quad (1) - (5) \\ \text{for } t' \in [t, \Psi(t)], (14), (15b), (15c), (19), (25). &\quad (26) \end{aligned}$$

Note that

$$\Phi(\mathcal{R}_P(t), \tau_P(t)) \leq \Phi^{(\kappa)}(\mathcal{R}_P(t), \tau_P(t))$$

and

$$\Phi(\mathcal{R}_P^{(\kappa)}(t), \tau_P^{(\kappa)}(t)) = \Phi^{(\kappa)}(\mathcal{R}_P^{(\kappa)}(t), \tau_P^{(\kappa)}(t)).$$

Moreover,

$$\Phi(\mathcal{R}_P^{(\kappa+1)}(t), \tau_P^{(\kappa+1)}(t)) < \Phi^{(\kappa)}(\mathcal{R}_P^{(\kappa)}(t), \tau_P^{(\kappa)}(t))$$

whenever  $\tau_P^{(\kappa+1)}(t) \neq \tau_P^{(\kappa)}(t)$  because  $\tau_P^{(\kappa+1)}(t)$  and  $\tau_P^{(\kappa)}(t)$  respectively are the optimal solution and a feasible point for (26). We thus arrive at

$$\begin{aligned} \Phi(\mathcal{R}_P^{(\kappa+1)}(t), \tau_P^{(\kappa+1)}(t)) &\leq \\ \Phi^{(\kappa)}(\mathcal{R}_P^{(\kappa+1)}(t), \tau_P^{(\kappa+1)}(t)) &< \\ \Phi^{(\kappa)}(\mathcal{R}_P^{(\kappa)}(t), \tau_P^{(\kappa)}(t)) &= \\ F(\mathcal{R}_P^{(\kappa)}(t), \tau_P^{(\kappa)}(t)), & \end{aligned}$$

implying that  $\tau_P^{(\kappa+1)}(t)$  is a better feasible point than  $\tau_P^{(\kappa)}(t)$  for (22). For a sufficiently large  $\mu > 0$ ,  $g(\tau_P^{(\kappa)}(t)) \rightarrow 0$  as well, yielding an optimal solution of MICP (17). A pseudo-code for this computational procedure is provided by Algorithm 1.

---

#### Algorithm 1 MICP Solver

---

*Initialization.* Choose a feasible point  $\tau_P^{(0)}(t)$  for (22) as the optimal solution of the following problem by relaxing the binary constraints (12) in (17) to box constraints:

$$\begin{aligned} \min_{W_P(t), \mathcal{R}_P(t), \tau_P(t)} \quad & F_P(\mathcal{R}_P(t), \tau_P(t)) \\ \text{s.t.} \quad & (14), (15b), (15c), (19). \end{aligned} \quad (27)$$

Set  $\kappa = 0$ .

$\kappa$ -th iteration. Solve (26). If the optimal solution  $\tau_P^{(\kappa+1)}(t)$  satisfies

$$\sum_{k_n \in \mathcal{C}(t)} \sum_{t'=t}^{t_{k_n, d}} \left( \tau_{k_n}^{(\kappa+1)}(t') - \left( \tau_{k_n}^{(\kappa+1)}(t') \right)^L \right) \approx 0,$$

terminate the algorithm and output  $\tau_P^{(\kappa+1)}(t)$  as a found solution. Otherwise, reset  $\kappa + 1 \rightarrow \kappa$  and  $\tau_P^{(\kappa+1)}(t) \rightarrow \tau_P^{(\kappa)}(t)$  for the next iteration.

---

### 3.2. Stage II: Computational procedure for (18)

To make the paper self-contained, the nonsmooth optimization Algorithm 2 [27, 26, 28], which computes solution of (18) via the following penalized optimization problem for  $\nu > 0$ :

$$\min_{W(t), R(t)} F(P_g(t)) + \nu(\text{Trace}(W(t)) - \lambda_{\max}(W(t))), \quad (28a)$$

$$\text{s.t.} \quad (18b), W(t) \succeq 0, \quad (28b)$$

is recalled here.

---

#### Algorithm 2 Nonsmooth optimization algorithm for (18)

---

*Initialization.* Choose a feasible point  $W^{(0)}(t)$  for (28). Set  $\kappa = 0$ .

$\kappa$ -th iteration. Solve

$$\begin{aligned} \min_{W(t), R(t)} \quad & F(P_g(t)) + \nu(\text{Trace}(W(t)) \\ & - (w_{\max}^{(\kappa)}(t))^H W(t) w_{\max}^{(\kappa)}(t)) \quad \text{s.t.} \end{aligned} \quad (28b), (29)$$

where  $w_{\max}^{(\kappa)}(t)$  denotes the normalized eigenvector corresponding to the maximal eigenvalue  $\lambda_{\max}(W^{(\kappa)}(t))$  of  $W^{(\kappa)}(t)$ . If the optimal solution  $W^{(\kappa+1)}(t)$  satisfies  $\text{Trace}(W^{(\kappa+1)}(t)) - (w_{\max}^{(\kappa+1)}(t))^H W^{(\kappa+1)}(t) w_{\max}^{(\kappa+1)}(t) \leq \epsilon$  for a given tolerance  $\epsilon > 0$  terminate the Algorithm and output  $V(t)$  such that  $V(t)V^T(t) = W^{(\kappa+1)}(t)$  as a found solution. Otherwise, reset  $\kappa + 1 \rightarrow \kappa$  and  $W^{(\kappa+1)}(t) \rightarrow W_P^{(\kappa)}(t)$  for the next iteration.

---

## 4. Lower bounding by offline computation

To investigate the optimality of the MPC-based online computation in the previous section, in this section we consider its offline counterpart, which uses the arrival and departure times of all PEVs during the entire charging period  $\mathcal{T}$  together with their charging states from the beginning in addressing for (11). Of course, such an offline computation cannot be implemented in practice but it provides a lower bound for the practically implemented online computation.

Similarly, the offline computation for (11) is of two following optimization stages. *Stage I.* The matrix rank-one constraints in (11c) are dropped to relax (11) to the MICP

$$\begin{aligned} \min_{W, \mathcal{R}, \tau} \quad & \mathcal{F}(\mathcal{R}, \tau) \quad \text{s.t.} \quad (1) - (5), (6), (8) - (10), \\ & W(t') \succeq 0, \quad \text{for } t' \in \mathcal{T}. \end{aligned} \quad (30)$$

which can be computed by Algorithm 1 with (26) for the  $\kappa$ -th iteration replaced by

$$\min_{W, \mathcal{R}, \tau} F(\mathcal{R}, \tau) + \mu \left( \frac{1}{g^{(\kappa)}(\tau)} - \frac{1}{\bar{\tau}} \right) \text{s.t.} \quad (1) - (5),$$

$$(8) - (10), W(t') \succeq 0, \tau_{k_n}(t') \in [0, 1], \quad \text{for } t' \in \mathcal{T}, \quad (31a)$$

$$L\tau_{k_n}(t') \geq (L-1)\tau_{k_n}^{(\kappa)}(t'), \quad \text{for } k \in \mathcal{C}, \quad (31b)$$

where  $g^{(\kappa)}(\tau) \triangleq \sum_{k \in \mathcal{G}} \sum_{k_n \in \mathcal{H}_k} \sum_{t'=t_{k_n, a}}^{t_{k_n, d}} (L\tau_{k_n}^{(\kappa)}(t'))^{L-1} \tau_{k_n}(t') - (L-1)\tau_{k_n}^{(\kappa)}(t')$ , and  $\bar{\tau} \triangleq \sum_{k \in \mathcal{G}} \sum_{k_n \in \mathcal{H}_k} \bar{\tau}_{k_n}$ .

*Stage II.* Suppose that  $\hat{W}$ ,  $\hat{\mathcal{R}}$  and  $\hat{\tau}$  are the found optimal solution of MICP (30). If  $\text{rank}(\hat{W}(t)) \equiv 1$ ,  $t \in \mathcal{T}$  then accept  $\hat{\mathcal{R}}$  and  $\hat{\nu}$  with  $\hat{V}(t)\hat{V}^H(t) = \hat{W}(t)$ ,  $t \in \mathcal{T}$  and  $\hat{\tau}$  as the optimal solution of (11). Otherwise, for those  $t \in \mathcal{T}$  with  $\text{rank}(\hat{W}(t)) > 1$  we substitute  $\hat{\tau}(t)$  to have (18) and use Algorithm 2 for its computation.

## 5. Simulation results

### 5.1. Setup

Sedumi[33] interfaced by CVX [34] on a Core i7-7600U processor is used to solve convex optimization problems such as (26), (29) and (31). The tested grid is a balanced distribution network modified from the IEEE 123 test feeder with the nominal voltage of 4.16 kV. Its details and data of system structure, physical limits and cost functions can be found in [35]. There are three distributed generators, which are respectively connected with buses 16, 36, 56, and ten charging stations have been randomly placed on buses 4, 7, 11, 17, 21, 28, 33, 40, 44 and 51.

The charging period is from 6:00 pm to 6:00 am of the next day to reflect the fact that most PEVs are charged after their owners' working hours. This time period is uniformly divided into 24 30-minute time slots [5]. The PEVs arrive during the time period from 6:00 pm to midnight. The arrival times of PEVs are independent and are generated by a truncated normal distribution  $(8, 1.5^2)$  [1, Fig.2]. There are three types of PEVs: normal PEVs, which are required to be fully charged by 6:00 am; median PEVs, which are required to be fully charged six hours after their arrivals; and urgent PEVs, which must be charged immediately when connected to grid. The randomly generated numbers of PEVs served at CSs are given in Table 1. There are totally 137 normal PEVs, 39 median PEVs and 23 urgent PEVs. The energy price for normal PEVs, median PEVs and urgent PEVs is  $\beta_t$ ,  $1.5\beta_t$  and  $2\beta_t$ , respectively, where the energy prices  $\beta_t$  of on May 17th, May 18th, May 19th and May 20th 2017 from 6:00 pm to 6:00 am are given in Fig.1.

The energy capacity of the EV batteries  $C_{k_n} = 50$  kWh is that of Tesla Model 3[36]. The initial SOC  $s_{k_n}^0$  in (11c) of all PEVs is set as 20%. The maximal charging power  $u_h \bar{P}_{k_n}$  per time slot is set to be equivalent to 10% of the battery capacity, i.e. every PEV needs to charge  $\bar{P}_{k_n}$  in 8 time slots. There are more than  $12!/8! = 990$  feasible on-off charges for each PEV, making the binary constraints in (11) combinatoric, which is too large to be handled by brute-force search.

The real price-inelastic demand  $P_{l_k}(t)$  is defined according to [37] as  $P_{l_k}(t) = \frac{l(t)}{\sum_{t=1}^{24} l(t)} \times \bar{P}_{l_k} T$ ,  $t \in \mathcal{T}$ , where  $\bar{P}_{l_k} T$  with the load demand  $\bar{P}_{l_k}$  indicates the total price-inelastic demand during the serving time period, while  $\frac{l(t)}{\sum_{t=1}^{24} l(t)}$  with the residential load demand  $l(t)$  at  $t$  indicates the proportion of price-inelastic demand at each time  $t$ . In our simulation, the data for  $\bar{P}_{l_k}$  is taken from by [35], while the data for  $l(t)$  is taken from [38]. The residential load demands  $l(t)$  on May 17th, May 18th, May 19th and May 20th 2017 from 6:00 pm to 6:00 am are plotted in Fig. 1.

The weighting factor  $\gamma = 10^3$  is set. The tolerance  $\epsilon = 10^{-3}$  is set for the stop criteria in the optimization algorithms.

### 5.2. Performance of the algorithms

The computational results are summarized in the fifth to seventh columns in Table 2, The effectiveness of using the online computation based on (18) is confirmed by observing that the computed sum of the energy cost to DGs and charging cost for PEVs is almost the same to its counterpart computed by the offline computation based on (11). The average running time of computation at each time slot is shown in the sixth column. Furthermore, Fig.2 indicates that Algorithm 1 for all profiles converge rapidly within several iterations.

The total power demand, the real price-inelastic demand, and the charging demand under Profile 1 are plotted in Fig. 3, while the three types of PEV charging demands under Profile 1 are shown in Fig. 4. It can be seen the price-inelastic demand reaches a peak value at 6:00 PM but then decreases continuously till midnight and remains low values from 0:00 am to 6:00 am. The total power demand  $P_{tot}(t)$  in real-time, which constitutes the real price-inelastic demand and total charging demand in real time, is stable during the serving time period. The fluctuation rate of the total power demand defined by  $\max\{\frac{\max_{t \in \mathcal{T}} P_{tot}(t) - P_{avg}}{P_{avg}}, \frac{P_{avg} - \min_{t \in \mathcal{T}} P_{tot}(t)}{P_{avg}}\}$  is within 7%. One can see that the magnitudes of the total demand are all around 2100 KW, while the charging demands are within 0-700 KW, so the PEVs' charging demand indeed is sizable enough to have a substantial impact to the grid operation. For other profiles, the results are similar.

The voltage magnitude during the serving time period under Profile 1 is shown in Fig. 5. The voltage magnitude starts to drop after 9:00 pm since most PEVs charge after that time but their values are always within the range of (1.165, 1.2] pu. This means that the impact of PEV penetration into the grid is well managed. Fig.6 plots the SoC of two normal PEVs and two median PEVs randomly taken from Profile 1, which arrive at different times. For a few time slots, PEVs do not charge so their SoC remain unchanged. The computational performance of the offline algorithm, which provides a lower bound for the online algorithm, and its comparison with the online counterpart are summarized in the last three columns of Table 2. The gap between online charging and offline charging costs is very light. Fig.7 plots SoC of a normal PEV and a median PEV randomly taken from profile 1, which are seen differently by online and offline algorithms though they result in similar values of the cost.

## 6. Conclusions

On-off PEV charging is very attractive thanks to its efficient online implementation, which is free from a mechanism to control the analog PEV charging values within battery capacity. The joint online coordination of PEV on-off charging and power control to serve both PEVs at a competitive cost and residential power demands at a competitive operating cost while managing the potential

Table 1: PEV number in each charging station during the charging period

CS #	4	7	11	17	21	28	33	40	44	51
Normal	14	12	14	14	15	12	13	15	13	15
Median	3	4	3	3	3	6	4	6	4	3
Urgent	3	2	2	3	3	2	3	1	1	3

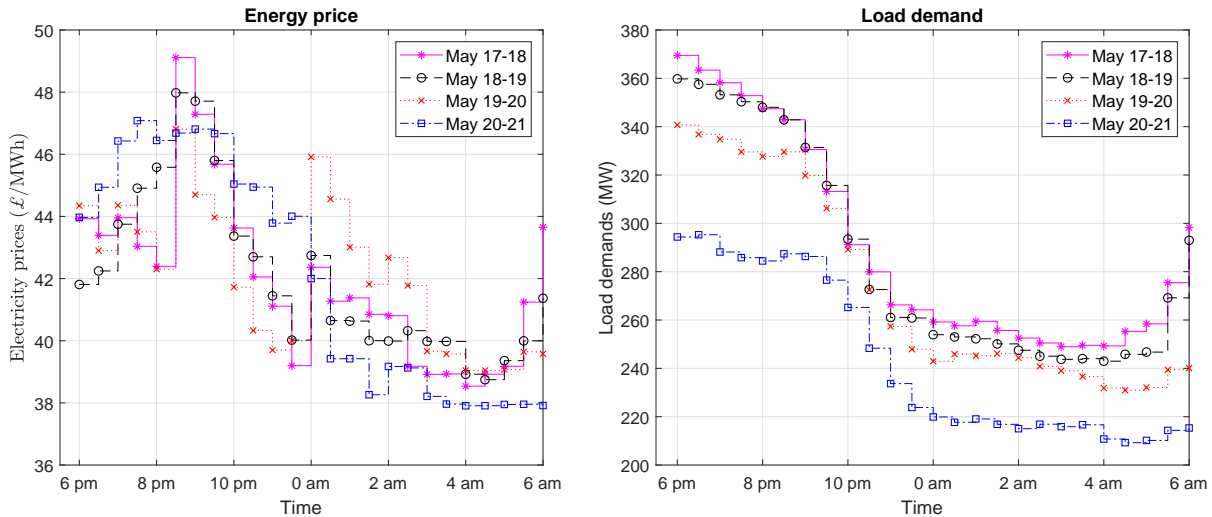


Figure 1: Energy price and residential load demand for four profiles

Table 2: Online and Offline computational results

Profile	# of binary Var.	$\mu$	$\nu$	Online computed cost	Avg. Time (s)	Offline computed cost	Diff.	Time (s)
1	3330	1	1	5712.06	104.7	5660.24	0.9%	172.5
2	3330	1	1	5717.29	108.2	5671.55	0.8%	162.3
3	3330	1	1	5591.97	97.6	5558.42	0.6%	151.1
4	3330	1	1	5651.39	110.5	5600.53	0.9%	160.4

of the power demand fluctuation is very difficult due to the random nature of PEVs' arrivals and demands and the combinatoric nature of on-off decisions. We have proposed a novel and easily-implemented MPC-based two-stage optimization online algorithm that can achieve an optimal solution.

## References

## References

- [1] Y. Shi, H. D. Tuan, A. V. Savkin, T. Q. Duong, H. V. Poor, Model predictive control for smart grids with multiple electric-vehicle charging stations, *IEEE Trans. Smart Grid* PP (99) (2018) 1–1.
- [2] Edison Electric Institute, Transportation electrification: Utility fleets leading the charge (white paper), EEI.
- [3] International Energy Agency, Global EV outlook 2016: Beyond one million electric cars, OECD/IEA.
- [4] N. Roterling, M. Ilic, Optimal charge control of plug-in hybrid electric vehicles in deregulated electricity markets, *IEEE Trans. Power Systems* 26 (3) (2011) 1021–1029.
- [5] C. Jin, J. Tang, P. Ghosh, Optimizing electric vehicle charging: A customer's perspective, *IEEE Trans. Veh. Tech.* 62 (7) (2013) 2919–2927.
- [6] Y. Wang, W. Saad, Z. Han, H. V. Poor, T. Basar, A game-theoretic approach to energy trading in the smart grid, *IEEE Trans. Smart Grid* 5 (3) (2014) 1439–1450.
- [7] L. Yang, J. Zhang, H. V. Poor, Risk-aware day-ahead scheduling and real-time dispatch for electric vehicle charging, *IEEE Trans. Smart Grid* 5 (2) (2014) 693–702.
- [8] Y. Wang, W. Saad, N. B. Mandayam, H. V. Poor, Load shifting in the smart grid: To participate or not?, *IEEE Trans. Smart Grid* 7 (6) (2016) 2604–2614.
- [9] S. Lakshminarayana, Y. Xu, H. V. Poor, T. Q. S. Quek, Cooperation of storage operation in a power network with renewable generation, *IEEE Trans. Smart Grid* 7 (4) (2016) 2108–2122.
- [10] E. Sortomme, M. M. Hindi, S. J. MacPherson, S. Venkata, Coordinated charging of plug-in hybrid electric vehicles to minimize distribution system losses, *IEEE Trans. Smart Grid* 2 (1) (2011) 198–205.
- [11] S. Huang, H. Safullah, J. Xiao, B.-M. S. Hodge, R. Hoffman, J. Soller, D. Jones, D. Dinger, W. E. Tyner, A. Liu, et al., The effects of electric vehicles on residential households in the city of indianapolis, *Energy Policy* 49 (2012) 442–455.
- [12] R. Verzijlbergh, C. B. Martinez-Anido, Z. Lukszo, L. de Vries, Does controlled electric vehicle charging substitute cross-border transmission capacity?, *Applied Energy* 120 (2014) 169 – 180.
- [13] Y. Li, C. Davis, Z. Lukszo, M. Weijnen, Electric vehicle charging in chinas power system: Energy, economic and environmental trade-offs and policy implications, *Applied Energy* 173 (2016) 535 – 554.
- [14] W. Liu, W. Hu, H. Lund, Z. Chen, Electric vehicles and large-

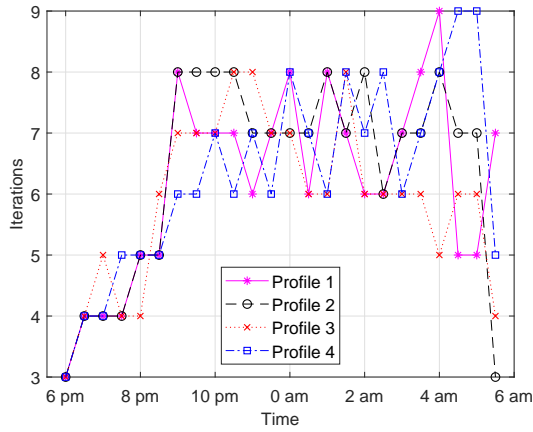


Figure 2: Iteration number of each time slot under four residential profiles

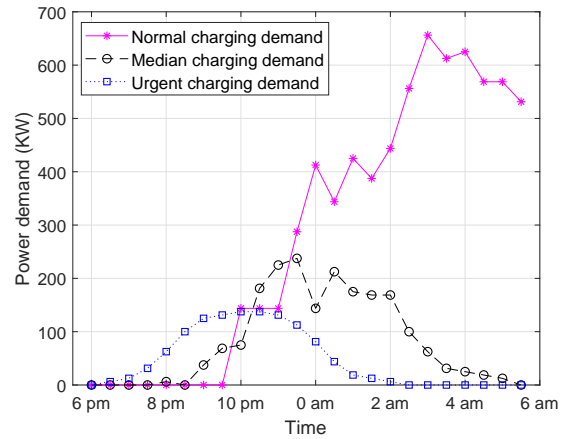


Figure 4: Three types of PEV charging demand under Profile 1 during the serving time period

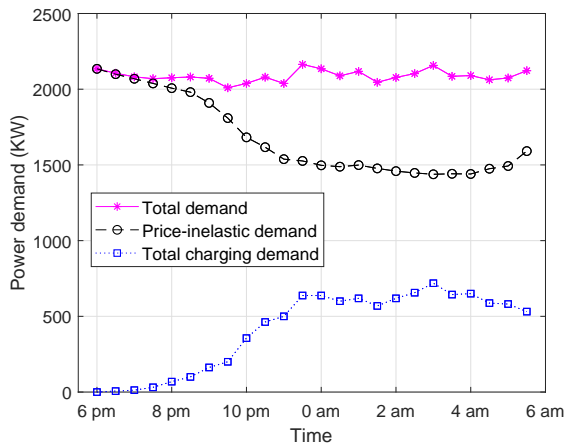


Figure 3: Total power demand, charging power demand and real price-inelastic demand under Profile 1 during the serving time period

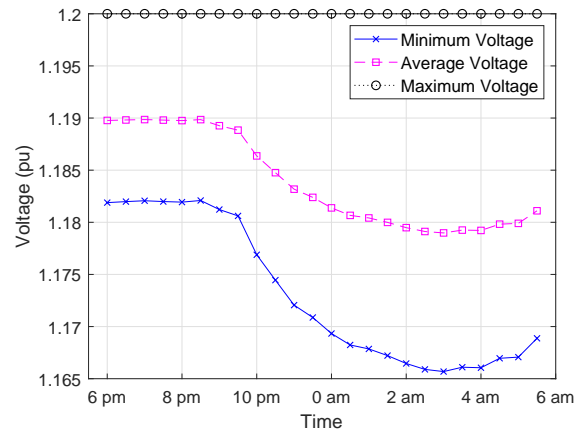


Figure 5: The voltage behavior under Profile 1 during the serving time period

scale integration of wind power the case of inner mongolia in china, *Applied Energy* 104 (2013) 445 – 456.

[15] E. Sortomme, M. A. El-Sharkawi, Optimal charging strategies for unidirectional vehicle-to-grid, *IEEE Trans. Smart Grid* 2 (1) (2011) 131–138.

[16] K. Clement-Nyns, E. Haesen, J. Driesen, The impact of vehicle-to-grid on the distribution grid, *Electric Power Systems Research* 81 (1) (2011) 185–192.

[17] H. Xing, M. Fu, Z. Lin, Y. Mou, Decentralized optimal scheduling for charging and discharging of plug-in electric vehicles in smart grids, *IEEE Trans. Power Syst.* 31 (5) (2016) 4118–4127.

[18] L. Hua, J. Wang, C. Zhou, Adaptive electric vehicle charging coordination on distribution network, *IEEE Trans. Smart Grid* 5 (6) (2014) 2666–2675.

[19] J. F. Franco, M. J. Rider, R. Romero, A mixed-integer linear programming model for the electric vehicle charging coordination problem in unbalanced electrical distribution systems, *IEEE Trans. Smart Grid* 6 (5) (2015) 2200–2210.

[20] C. S. Antnez, J. F. Franco, M. J. Rider, R. Romero, A new methodology for the optimal charging coordination of electric vehicles considering vehicle-to-grid technology, *IEEE Trans. Sustainable Energy* 7 (2) (2016) 596–607.

[21] W. Tang, Y. J. A. Zhang, A model predictive control approach for low-complexity electric vehicle charging scheduling: optimality and scalability, *IEEE Trans. Power Systems* 32 (2) (2017)

1050–1063.

[22] P. Malysz, S. Sirouspour, A. Emadi, An optimal energy storage control strategy for grid-connected microgrids, *IEEE Trans. Smart Grid* 5 (4) (2014) 1785–1796.

[23] A. Ravichandran, S. Sirouspour, P. Malysz, A. Emadi, A chance-constraints-based control strategy for microgrids with energy storage and integrated electric vehicles, *IEEE Trans. Smart Grid* 9 (2018) 346–359.

[24] E. F. Camacho, C. Bordons, *Model Predictive Control*, Springer-Verlag, Springer, 2004.

[25] A. Mesbah, *Stochastic model predictive control: An overview and perspectives for future research*, *IEEE Control Systems Mag.* 36 (6) (2016) 30–44.

[26] Y. Shi, H. D. Tuan, H. Tuy, S. Su, Global optimization for optimal power flow over transmission networks, *J. Global Optimiz.* 69 (3) (2017) 745–760.

[27] A. H. Phan, H. D. Tuan, H. H. Kha, D. T. Ngo, Nonsmooth optimization for efficient beamforming in cognitive radio multicast transmission, *IEEE Trans. Sign. Process.* 60 (6) (2012) 2941–2951.

[28] Y. Shi, H. D. Tuan, A. V. Savkin, Global optimal power flow over large-scale power transmission networks, *Systems & Control Letters* 118 (1) (2018) 16–21.

[29] E. Che, H. D. Tuan, H. H. Nguyen, Joint optimization of cooperative beamforming and relay assignment in multi-user wireless

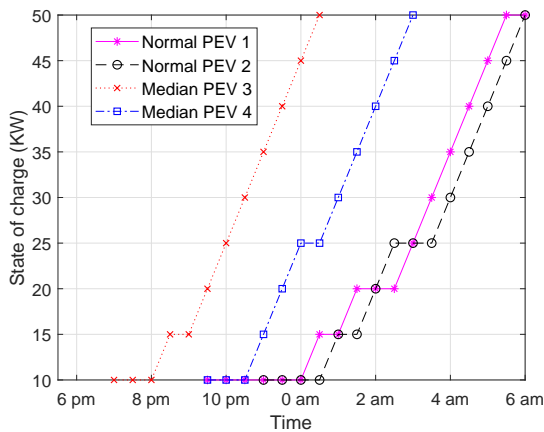


Figure 6: The SoC of PEVs under Profile 1 during the serving time period

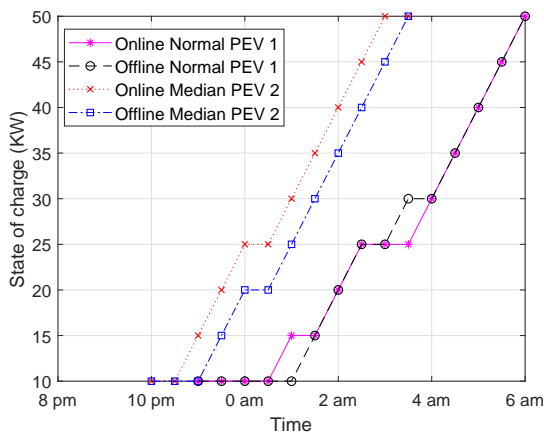


Figure 7: SoC of PEVs by online and offline charging under Profile 1 during the serving time period

relay networks, *IEEE Trans. Wirel. Commun.* 13 (10) (2014) 5481–5495.

[30] H. H. M. Tam, H. D. Tuan, D. T. Ngo, T. Q. Duong, H. V. Poor, Joint load balancing and interference management for small-cell heterogeneous networks with limited backhaul capacity, *IEEE Trans. Wirel. Commun.* 16 (2) (2017) 872–884.

[31] H. Tuy, *Convex Analysis and Global Optimization* (second edition), Springer International Publishing AG, 2017.

[32] J. F. Bonnans, J. C. Gilbert, C. Lemarechal, C. Sagastizabal, *Numerical Optimization Theoretical and Practical Aspects*, 2nd Edition, Springer, 2006.

[33] J. Sturm, Using SeDuMi 1.02, a MATLAB toolbox for optimization over symmetric cones, *Optimization Methods and Software* 11–12 (1999) 625–653.

[34] M. Grant, S. Boyd, CVX: Matlab software for disciplined convex programming, version 2.1, <http://cvxr.com/cvx> (Mar. 2014).

[35] S. Bolognani, Approximate linear solution of power flow equations in power distribution networks, 2014 [Online]. Available: <http://github.com/saveriob/approx-pf>.

[36] Tesla model 3, [https://en.wikipedia.org/wiki/Tesla\\_Model\\_3](https://en.wikipedia.org/wiki/Tesla_Model_3), accessed: 2017-08-17.

[37] N. Chen, C. W. Tan, T. Q. Quek, Electric vehicle charging in smart grid: Optimality and valley-filling algorithms, *IEEE J. Sel. Topics Signal Process.* 8 (6) (2014) 1073–1083.

[38] The residential demand of the UK, <http://www.gridwatch.templar.co.uk/download.php>, accessed: 2017-08-17.